Journal of Magnetic Resonance 199 (2009) 10–17

Contents lists available at ScienceDirect

Journal of Magnetic Resonance

journal homepage: www.elsevier.com/locate/jmr

Tunnelling magnetic resonances: Dynamic nuclear polarisation and the diffusion of methyl group tunnelling energy

A.J. Horsewill *, C. Sun

School of Physics & Astronomy, University of Nottingham, University Park, Nottingham NG7 2RD, UK

ARTICLE INFO

Article history:
Received 23 December 2008
Revised 19 March 2009
Available online 5 April 2009

Keywords:
Tunnel resonance
Field-cycling NMR
Dynamic nuclear polarisation
Methyl tunnelling
Tunnel diffusion

ABSTRACT

The dynamic nuclear polarisation (DNP) of ^{1}H spins arising from methyl tunnelling magnetic resonances has been investigated in copper-doped zinc acetate dihydrate using field-cycling NMR spectroscopy at 4.2 K. The tunnel resonances appear in the field range 20–50 mT and trace out the envelope of the electron spin resonance spectrum of the Cu^{2+} ion impurities. By investigating the DNP line shapes as a function of time, the cooling of the methyl tunnel reservoir has been probed. The role of spectral diffusion of tunnelling energy in determining the DNP line shapes has been investigated through experiments and numerical simulations based on a theoretical model that describes the time evolution of the ^{1}H polarisation and the tunnelling temperature. The model is discussed in detail in comparison with the experiments. All effects have been studied as a function of Cu^{2+} ion concentration.

1. Introduction

There has been much interest in recent years in utilising the phenomenon of dynamic nuclear polarisation (DNP) [1] for enhancing the polarisation of nuclear spins and thereby substantially improving NMR signals [2–4]. The investigation of DNP raises some interesting issues, notably in the context of the current investigation, the physics underpinning the transfer of energy between weakly coupled thermal reservoirs associated with the various spin systems. When molecular rotations are involved, the Pauli Exclusion Principle can have an important role to play in these processes since the requirements of antisymmetry for identical Fermions can impose strict constraints on the allowable eigenfunctions and the ways in which space and spin sub-systems can interact. A classic example is of *ortho*- and *para*-hydrogen wherein conversion between the two nuclear spin isomers is mediated by simultaneous changes in spatial and spin degrees of freedom. This requires fluctuating magnetic interactions that couple space and spin variables, for example the dipole–dipole interaction coupling the magnetic moments associated with particle spins. Photons or phonons alone do not have the required characteristics. Therefore, the coupling between such thermal reservoirs can often be weak so that energy is stored inside when the samples are cooled. Experimental procedures must be specially developed to facilitate contact and to enable the stored energy to flow into spin reservoirs of interest thereby generating nuclear polarisation.

The quantum tunnelling of methyl groups provides another example of the effect of the Pauli Exclusion Principle on the spatial and nuclear spin degrees of freedom. The methyl rotor, CH_3, experiences a potential barrier to rotation. This in general has threefold symmetry and the ground torsional state is split by a tunnelling splitting, $\hbar\omega_t$, separating two nuclear spin-symmetry species labelled *A* and *E*. The total wavefunction must be antisymmetric with respect to proton exchange among the three hydrogen atoms so that it transpires the *A* species is a nuclear spin quartet with a total spin $I = \frac{3}{2}$ while there are degenerate E_a and E_b species each of which are nuclear spin doublets with a total spin $I = \frac{1}{2}$. *A*–*E* conversion is therefore spin-symmetry restricted, moreover it is a resonant process requiring energy quanta $\hbar\omega_t$. As a result molecular crystals containing methyl groups possess 'tunnelling reservoirs' associated with the *A* and *E* nuclear spin-symmetry species which are thermally isolated from the lattice, particularly at low temperature. Consequently, following cooling of the sample, the tunnelling reservoir is characterised by a temperature θ_t that can remain significantly higher than the lattice temperature for many hours, days or even weeks.

The phenomenon of methyl tunnelling has been investigated using a variety of novel experimental techniques [5]. Among these is the family of 'tunnelling magnetic resonance' experiments whereby contact is made between the tunnelling reservoir and the Zeeman reservoir associated with either an electron or a nuclear spin by tuning the magnetic field [6–8]. When the Larmor frequency matches ω_t resonant contact is made, time-dependent interactions coupling space and spin become available to induce *A*–*E* conversion and as the energy flows, anomalies in the nuclear spin polarisation or relaxation properties are observed as 'tunnel

* Corresponding author. Fax: +44 (0) 115 9515180.
E-mail address: a.horsewill@nottingham.ac.uk (A.J. Horsewill).

1090-7807/$ - see front matter © 2009 Elsevier Inc. All rights reserved.
doi:10.1016/j.jmr.2009.03.013

resonances'. Therefore, methyl tunnelling is revealed in the magnetic field dependence of nuclear spin polarisation. A variety of tunnel resonance experiments have been reported in the literature and are reviewed in [8]. Of particular interest here are those investigations that probe the mechanisms of *A*–*E* conversion. Using NMR-type tunnel resonances the saturation techniques of Bharaj and Pintar [9] were adapted by the group of Van Gerven [10] to determine the *A*–*E* conversion time. For ESR-type tunnel resonances, where electron spins are brought into resonant contact with the tunnelling methyl groups, significant DNP effects on the proton spins can be observed as energy cascades out of the tunnel reservoir and redistributes itself through various pathways into the lattice. The mechanisms were originally described in a series of papers by Clough and co-workers [11–16]. In this paper we revisit the electron spin tunnel resonance phenomenon with new experiments designed to investigate the mechanisms underlying the creation of the DNP signal of the proton spins. The experiments reveal some interesting effects that originate from the Pauli Exclusion Principle and its effect on the combined space–spin eigenfunctions that characterise the sample.

Field-cycling NMR spectroscopy [17] provides an effective technique for investigating magnetic field-dependent tunnel resonance phenomena. In Section 3 a range of tunnel resonance experiments that reveal dynamic nuclear polarisation of ^{1}H spins are described. In Section 4 a theoretical model based on the principles established by Clough is summarised describing the changes in ^{1}H polarisation which occur when tunnelling methyl groups undergo a change in nuclear spin-symmetry; this analysis reveals the importance of a tunnel diffusion mechanism that acts to equilibrate the tunnelling temperature across an inhomogenously broadened distribution of tunnelling frequencies. In Section 5 the theoretical model is confronted with the experimental data through numerical simulations.

2. Experimental

The experiments have been conducted on single crystals of zinc acetate dihydrate in which the metal ions have been doped with small quantities of copper. The electron spin resonance (ESR) spectrum of the Cu^{2+} ions in this material is known from the literature [18]. The crystals were grown by slow evaporation of an aqueous solution of zinc and copper acetate. Three samples were studied with different copper ion concentrations. These were prepared from aqueous solutions with Cu:Zn mole ratios of: sample I, 5.2 mol%; sample II, 1.80 mol%; sample III, 0.78 mol%. The crystal axes were determined from the crystal morphology and the single crystals were aligned such that the axis of the applied magnetic field was oriented parallel to the *c*-axis that is close to the major principle axis of the *g*-tensor, $g_{//}$.

The NMR measurements were made using the Nottingham field-cycling NMR spectrometer [19]. The magnet system comprises a superconducting solenoid with low inductance (23 mH) that can provide a maximum *B*-field of 2.5 T with the facility to ramp the field at a rate of 10 T s^{-1}. The rapid switches in magnetic field are adiabatic enabling the nuclear spin polarisation to be explored as a function of magnetic field. The ^{1}H NMR signal was monitored using a TecMag Apollo pulsed NMR spectrometer. A typical field-cycling pulse sequence is shown in Fig. 1 where the ^{1}H spins are first saturated on resonance using a comb of $\pi/2$ pulses. The magnetic field is then rapidly switched to the relaxation field B_r where the system is allowed to evolve for the time τ_{rec} before being switched back to resonance where the ^{1}H polarisation is measured with a $\pi/2$ pulse. To plot a spectrum as a function of magnetic field, the sequence is repeated with systematic increments in B_r.

The magnet system is situated in a liquid helium cryostat and incorporates a variable temperature insert for the sample. All experiments were conducted at 4.2 K.

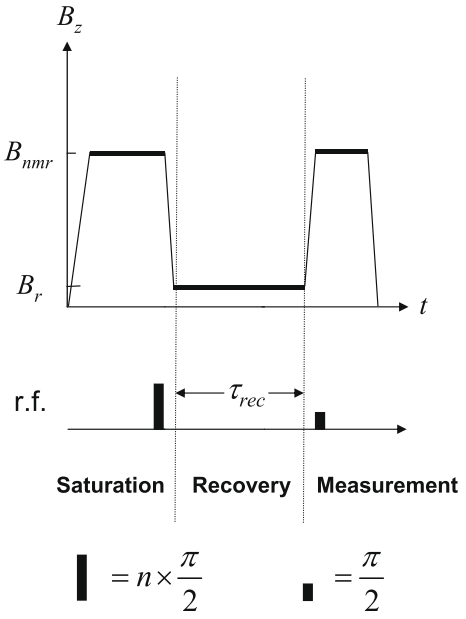

Fig. 1. The field-cycling NMR pulse sequence employed to study methyl tunnel resonances.

3. Tunnel resonance

3.1. Tunnel resonance spectra

Tunnel resonance spectra recorded on single crystals of (Cu,Zn) acetate dihydrate at 4.2 K are presented in Fig. 2. These record the ^{1}H spin polarisation as a function of relaxation field B_r and the three spectra were recorded on samples I, II and III possessing different copper ion concentrations. The time spent at the relaxation field was $\tau_{rec} = 60$ s and the spectra were recorded in the direction of decreasing field.

The ^{1}H polarisation exhibits strong, resonant deviations from thermal equilibrium in the region 20–50 mT. Each spectrum comprises four lines. The line shapes have the appearance of the (inverse) derivative of an absorption line so that on the high-field

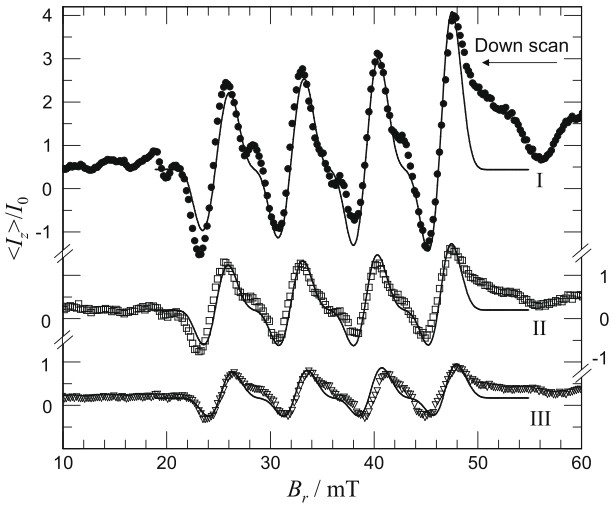

Fig. 2. Tunnel resonances recorded on Cu^{2+}-doped zinc acetate dihydrate. Down-field scans; $T = 4.2$ K, $\tau_{rec} = 60$ s. Sample I (filled circles); sample II (squares); sample III (triangles). The solid lines indicate the numerical simulations using the parameters given in Table 1, see text for details.

side the ^{1}H polarisation is enhanced, reflecting a cooling of the ^{1}H Zeeman reservoir, whereas on the low-field side the ^{1}H polarisation is reduced. In fact on the low-field side the nuclear polarisation becomes inverted indicating a substantial increase in the energy of the ^{1}H Zeeman reservoir. These line shapes are characteristic of DNP.

The ^{1}H polarisation $\langle I_z\rangle$ is plotted as a fraction of the equilibrium polarisation $I_0^{(B=35.9\ \mathrm{mT})}$ that characterises the system in the field $B = 35.9$ mT at the centre of the tunnel resonance spectrum. $I_0^{(B=35.9\ \mathrm{mT})}$ was determined for each sample from calibrations measuring the equilibrium proton polarisation at the field $B = 87$ mT which lies above the tunnel resonance spectrum. $\langle I_z\rangle/I_0^{(B=35.9\ \mathrm{mT})}$ is plotted in all the spectra in this report.

The tunnel resonance spectrum traces the envelope of the ESR spectrum of Cu^{2+} and the four-line spectrum arises from the hyperfine interaction between the unpaired electron on the Cu ion and the spin $I_{Cu} = \frac{3}{2}$ of the Cu nuclei. In the background further lines are evident which are assigned to paramagnetic manganese ion impurities in the sample; these will be disregarded.

The centre of the four-line spectrum represents the field B_{tr} at which the methyl tunnelling frequency matches the electron spin Larmor frequency;

$$\omega_t = g_{obs}\beta B_{tr}/\hbar \quad (1)$$

The methyl tunnelling frequency, $\omega_t = 7.52 \times 10^9\ \mathrm{s}^{-1}$, is known from inelastic neutron scattering [11] so with $B_{tr} = 35.9$ mT we obtain $g_{obs} = 2.38$ which is consistent with the orientation of the crystal in the magnetic field given the known g-tensor [18]. In this crystal orientation the copper hyperfine splitting is approximately 7.25 mT which is also consistent with the published ESR parameters [18].

When the sample was cooled from room temperature to 4.2 K, the methyl tunnelling reservoir became decoupled from the lattice and it is therefore characterised by a temperature that is higher than the lattice temperature. The tunnel resonance phenomenon occurs when resonant contact is made between the warm tunnel reservoir and the electron spin Zeeman reservoir. The latter, with efficient coupling to the lattice, is cold, so when an ESR frequency matches ω_t, electron–proton dipolar interactions become available to mediate the transfer of energy from the tunnel reservoir into the lattice. Since protons are involved, the process is accompanied by energy-conserving proton spins flips that polarise the ^{1}H spins. Substantial changes in proton polarisation can be maintained because the ^{1}H spin–lattice relaxation time is very long. We shall return later to investigate the mechanism in detail.

The direction of the field scan reveals hysteresis in $\langle I_z\rangle$. In Fig. 3 up-field and down-field scans on sample II are presented. Beginning with a freshly cooled sample the down-field scan was completed first (filled triangles), followed by the up-field scan (open squares). Comparing the two scans the hysteresis manifests itself in a number of ways (i) the centres of the derivative-shaped lines are offset and (ii) the DNP line shapes are asymmetric such that the positive lobes have higher amplitude in the down-field scan but the negative lobes have greater amplitude in the up-field scan. Fig. 3 shows the sum and difference of the up-field and down-field scans which have been calculated; the sum possesses more symmetric DNP line shapes (open triangles) whereas the line shapes in the difference appear Gaussian-like (open circles). A detailed interpretation of these line shapes will be discussed in a later section.

The baselines of the tunnel resonance spectra shown in Fig. 2 vary systematically with Cu^{2+} ion concentration. We can identify two mechanisms contributing to the baseline (i) spin–lattice relaxation and (ii) polarisation of the ^{1}H spins during the rapid field switches. The spin–lattice relaxation time is dependent on the Cu^{2+} ion concentration. Furthermore, to arrive at the lower magnetic field values, the technique encounters tunnel resonances during the field-cycling switches. Both mechanisms contribute to the baseline in a way that depends systematically on Cu^{2+} ion concentration.

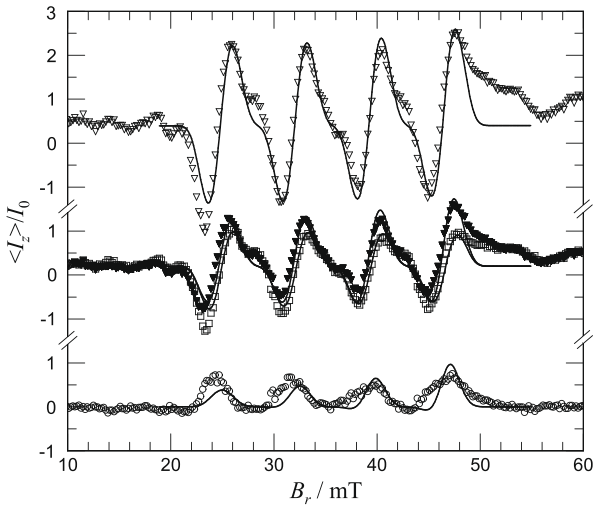

Fig. 3. Down-field scan (filled triangles) and up-field scan (squares) on sample II showing the hysteresis. Difference spectrum (open triangles) and sum spectrum (circles) are also shown together with the numerical simulations (solid lines).

3.2. The cooling of the tunnel reservoir

The heat capacity of the tunnelling reservoir is finite and by making repeated contact with the electron the reservoir will systematically lose energy and will cool. This effect is evident in Fig. 2 where, in a down-field scan on sample I with the highest Cu^{2+} ion concentration, the amplitudes of each of the four Cu hyperfine lines become successively smaller as the scan progresses. With more Cu^{2+} ions to relax the tunnel reservoir the rate of cooling is faster; therefore as the scan progresses the temperature gradient across the tunnelling and electron Zeeman reservoirs diminishes, systematically reducing the ^{1}H polarisation generated by the DNP effect. This effect is much diminished in sample III with the lowest Cu^{2+} ion concentration where the four lines have similar amplitude.

The cooling process has been monitored systematically in a series of experiments. Beginning with a freshly cooled sample, the tunnel resonance pulse sequence was employed repeatedly to record the ^{1}H polarisation generated at the fixed relaxation field B_r during the period $\tau_{rec} = 300$ s. In two sets of experiments B_r was chosen to coincide with either the positive or the negative lobe of the derivative-shaped DNP line belonging to the highest field member of the four Cu hyperfine components. The three samples I, II and III were investigated. The results are shown in Fig. 4 and each scan involved total contact times with the electron extending to more than 20 h. The amplitude of the DNP signal is larger for the samples with the higher Cu^{2+} ion concentration since more resonant centres are available to cool the tunnel reservoir. For each sample the ^{1}H polarisation generated on both positive and negative lobes of the DNP signal reduces systematically with time as the tunnelling reservoir cools.

The cooling is dominated by the contact with the electron so when the magnetic field is non-resonant the tunnel reservoir is strongly decoupled from the lattice and any relaxation time constants characterising the tunnel reservoir are likely to be in excess of many weeks at liquid helium temperatures. For practical reasons this non-resonant tunnelling relaxation rate has not yet been measured. On tunnel resonance, the DNP signal recovers towards the ^{1}H equilibrium polarisation in the limit of long time. When B_r coin-

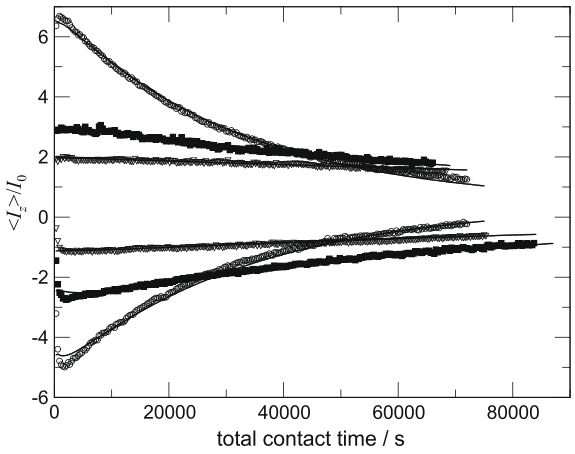

Fig. 4. The cooling of the tunnel reservoir recorded by monitoring the negative and positive lobes of the DNP line shape; $\tau_{rec} = 300$ s. Sample I (open circles); sample II (squares); sample III (triangles). Solid lines: numerical simulation.

cides with the negative lobe of the DNP signal, the ^{1}H polarisation approaches this equilibrium value from the direction of negative polarisations. Conversely, when the field is set to coincide with the positive lobe, the ^{1}H polarisation is always positive. In both cases the cooling follows an exponential recovery towards equilibrium,

$$\langle I_z \rangle = A \exp(-\tau/T_{tunn}) + I_0 \qquad (2)$$

where A is the ^{1}H polarisation generated by contact with the electron during 300 s for a freshly cooled sample. For each sample the characteristic time constants T_{tunn} recorded on each lobe have similar values: for sample I, $T^+_{tunn} \approx 3.2 \times 10^4$ s for the positive lobe and $T^-_{tunn} \approx 3.3 \times 10^4$ s for the negative lobe; sample II, $T^+_{tunn} \approx 1.0 \times 10^5$ s and $T^-_{tunn} \approx 0.9 \times 10^5$ s; sample III, $T^+_{tunn} \approx 1.9 \times 10^5$ s and $T^-_{tunn} \approx 2.1 \times 10^5$ s. It is clear that for samples with larger Cu^{2+} ion concentration the cooling rate is faster and the initial DNP magnitude is larger.

3.3. Tunnel diffusion

Conventionally, the difference in frequency between the negative and positive lobes of a derivative-shaped DNP signal is equal to twice the ^{1}H Larmor frequency, $2\omega_n$. Consider the widths of the tunnel resonance line shapes shown in Fig. 2. The difference in magnetic field between the negative and positive lobes is approximately 2.5 mT which is equivalent to 83 MHz in frequency units. This is substantially larger than the value $2\omega_n = 3.1$ MHz corresponding to the field value at the centre of the tunnel resonance spectrum. It is also significantly broader than the inherent ESR linewidth of 21 MHz (0.63 mT) [18]. Furthermore, the breadth of the four DNP peaks of the tunnel resonance spectrum is independent of magnetic field, despite the field dependence of ω_n which varies by a factor of approximately two across the spectrum. Therefore, it is evident that the DNP line shapes have excess width and this is attributable to the inherent linewidth of the tunnelling spectrum of the methyl groups. In fact, the tunnelling frequency is inhomogenously broadened reflecting a distribution of tunnelling frequencies in the sample. This has important consequences since the diffusion of tunnelling energy amongst the tunnelling distribution provides an additional mechanism for the creation of dynamic nuclear polarisation. Supporting evidence for the diffusion of tunnelling energy through the crystal comes from the initial few points at the beginning of each scan shown in Fig. 4; these reveal some hysteresis and are reminiscent of related tunnel diffusion effects observed by Clough et al. [12].

The tunnelling energy spectrally and spatially diffuses among the methyl groups in the crystal. When there is a mismatch between the frequencies of two CH_3 groups they can still exchange a quantum of tunnelling energy so long as the process is accompanied by a change in a ^{1}H spin state so that the energy mismatch is made up by a quantum of ^{1}H Zeeman energy. On the high-field side of the resonance there is a net cooling of the ^{1}H Zeeman reservoir leading to an enhancement of the ^{1}H polarisation whereas on the low-field side there is a net warming of the ^{1}H Zeeman reservoir leading to an inversion of the ^{1}H polarisation as shown in Fig. 2. This is the signature of a DNP process and the 'Tunnel Diffusion' mechanism makes a significant contribution to the observed tunnel resonance line shapes.

The tunnel diffusion rate has been measured in the following way; the magnetic field was initially set to tunnel resonance on the positive lobe of a DNP line shape. Here the system was prepared by evolving for a time $\tau_{rec} = 1800$ s during which energy flowed out of the tunnel reservoir due to contact with the electron spin. Following this preparation period the ^{1}H polarisation recovering in the time $\tau_{rec} = 10$ s at the field $B_r \approx 84$ mT was repeatedly measured using the field-cycling saturation-recovery sequence shown in Fig. 1, the ^{1}H polarisation having been reduced to zero after each measurement. Following the initial contact, no further contact with the tunnel resonance spectrum was made throughout the experiment. The results are presented in Fig. 5; even though B_r was offset from the tunnel resonance so that the electron was non-resonant, $\langle I_z \rangle$ has an initial magnitude that is significantly larger than that which would have recovered due to spin–lattice relaxation alone. Subsequent measurements display a decay with time towards equilibrium. When the field during the preparation period was set to the negative lobe of the DNP line shape, Fig. 5, the initial ^{1}H polarisation was inverted. Subsequent measurements display a growth towards equilibrium. These results are explained as follows: following contact with the electron, energy flows out of the tunnel reservoir. The system is disturbed away from its pseudo-equilibrium state and the energy is redistributed via tunnel diffusion, resulting in changes in the ^{1}H polarisation. Even though the field is no longer set to tunnel resonance, DNP continues to be generated for a period of approximately 100 s.

From the data given in Fig. 5 we were able to measure the decay time constant characterising the tunnel diffusion process. This is approximately $T_{diff} = 25$ s. Given the mechanism does not involve the electron spins we do not expect a strong dependence of the diffusion time constant on the Cu^{2+} ion concentration; qualitatively

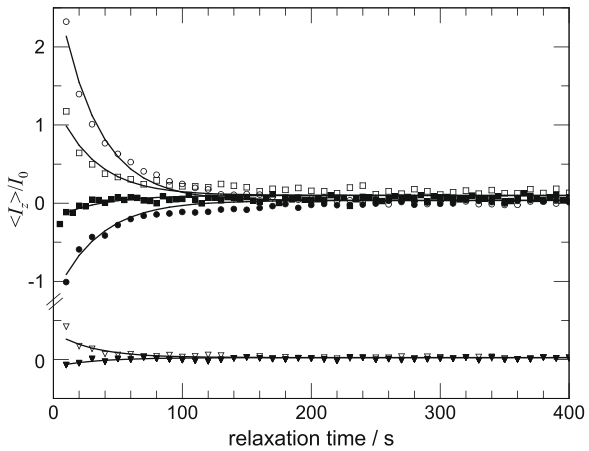

Fig. 5. Effects of tunnel diffusion recorded on: sample I (circles); sample II (squares); sample III (triangles, offset by $\langle I_z \rangle / I_0 = -2$ for clarity). Preparation $\tau_{rec} = 1800$ s on tunnel resonance: then $\langle I_z \rangle$ monitored every 10 s off tunnel resonance at $B_r = 84$ mT. Solid lines: numerical simulation.

this seems to be the case in measurements on the three different samples, Fig. 5.

3.4. Time evolution at the tunnel resonance

The build-up of the DNP signals as a function of time has been investigated in a series of saturation-recovery measurements. In a sequence that is reminiscent of one designed to measure spin–lattice relaxation, $\langle I_z \rangle$ has been measured as a function of recovery time τ_{rec}, at the fixed field B_r which coincided with either the positive or negative lobe of the DNP signal. In each sequence of measurements logarithmic increments in time were selected. The experiments were conducted on the three samples I, II and III and each sequence was started with a freshly cooled sample. The scan was conducted systematically beginning with short recovery times and the results are presented in Fig. 6. The DNP signal initially builds up approaching values some 4–7 times the equilibrium polarisation. A maximum is encountered after contact times of 1000–7000 s depending on Cu^{2+} ion concentration whereupon the polarisation subsequently decays towards equilibrium.

There are a variety of mechanisms to consider (a) the generation of the DNP signal through contact between the tunnelling reservoir and the electron spin; (b) tunnel diffusion; (c) the systematic cooling of the tunnel reservoir; (d) the spin–lattice relaxation of the protons. The maximum in polarisation is greatest for the highest Cu^{2+} ion concentration but due to the more rapid cooling of the tunnel reservoir and the faster T_1 value, the DNP signal also decays more quickly than that of the samples with lower concentration. The spin–lattice relaxation time was also measured by recording the polarisation recovery at a non-resonant field value $B_r = 89$ mT such that the tunnel resonance was not encountered in the field-cycling scan used to record the data, and is shown in Fig. 6. The T_1 values are dependent on the Cu^{2+} ion concentration and are reported in Table 1. With values of order 1000–3000 s they are consistent with the recovery times that characterise the peaks in the tunnel resonance curves shown in Fig. 6.

4. DNP model for tunnel resonance including tunnel diffusion

The principles underlying the phenomenon of methyl tunnel resonance have been treated in a number of papers by Clough [12–16]. Using these as a basis we shall develop a model for DNP from which numerical simulations of the tunnel resonance DNP line shapes can be developed, culminating in fits to our experimental data.

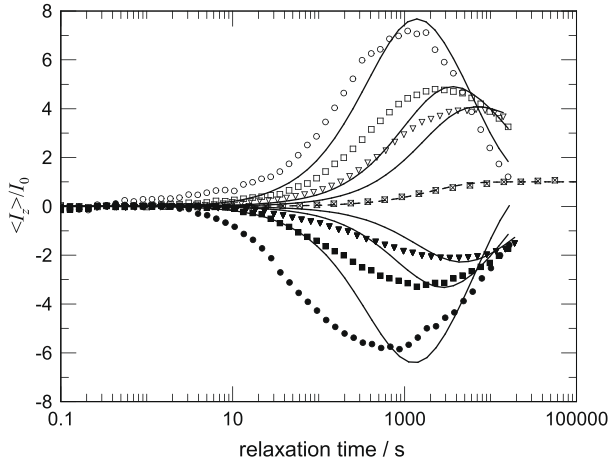

Fig. 6. The time evolution of the tunnel resonance: sample I (circles); sample II (squares); sample III (triangles). Solid lines: numerical simulation. The non-resonant magnetisation recovery at $B_r = 89$ mT for sample II; ⊠ and dashed line (fit).

Table 1
Experimental and best fit parameters describing the tunnel resonance spectra and the numerical simulations.

	Sample I	Sample II	Sample III
(Cu:Zn) ratio	1:18.2	1:54.5	1:218
Cu^{2+} concentration, C	5.2 mol%	1.80 mol%	0.78 mol%
T_1 (48 mT) (s)	600	1200	1800
T_1 (89 mT) (s)	1010	2140	2890
$aW^{(+)} = aW^{(-)}$ ($K\,s^{-3}$)	4.4×10^{16}	1.8×10^{16}	0.9×10^{16}
$a_t W^{(-)} = a_t W^{(+)} = a_t W^{(0)}$ (s^{-3})	2×10^{13}	0.7×10^{13}	0.35×10^{13}
k_d (s^{-1})	0.04	0.04	0.04
k_0 ($s^{-2}\,K^{-1}$)	2.25×10^9	2.25×10^9	2.25×10^9

$g_{obs} = 2.38, A_{Cu} = 7.25$ mT, $\omega_t = 7.25 \times 10^9$ s^{-1}, $b = 1.9 \times 10^8$ s^{-1}.

The crystal contains methyl groups with mean tunnelling frequency ω_t. There is a Gaussian distribution of frequencies $G(\omega_t^{(i)}) = \frac{1}{b\sqrt{2\pi}} \exp(-\frac{1}{2}((\omega_t^{(i)} - \omega_t)/b)^2)$ about this mean so that the tunnel frequency of a subgroup labelled i is $\omega_t^{(i)}$ and b is the half width at half maximum (HWHM) of the distribution. A thermal reservoir with temperature $\theta_{t(i)}$ is associated with each subgroup i; these are only very weakly coupled to the lattice, particularly at low temperature, so that on cooling the sample $\theta_{t(i)}$ becomes decoupled from the lattice temperature θ_L. The tunnel reservoir retains its energy, remaining hotter than the lattice so that non-equilibrium populations will characterise the A and E spin-symmetry species. The tunnelling subgroups are however coupled among themselves and equilibrate via the tunnel diffusion mechanism towards a common tunnelling temperature.

The paramagnetic Cu^{2+} ions are randomly distributed in the crystal and are characterised by the ESR spectrum $g(\omega)$. This spectrum is governed by the electron spin Zeeman interaction with the applied field B and the hyperfine interaction with the Cu nucleus of spin 3/2 (coupling constant A_{Cu}). Therefore, the electron spin resonance frequency is determined by $\omega_s = g_{obs}\beta B/\hbar + A_{Cu} m_I^{Cu}$.

In a tunnel resonance experiment the electron spins will be in resonance with methyl groups i when $\omega_s = \omega_t^{(i)}$. However, matching the energy quanta on its own is not a sufficient condition for mediating the transfer of energy from the tunnel reservoir to the electron spins. Transitions in methyl tunnelling state involve changes in nuclear spin-symmetry species. Therefore, in this context, only the electron–nuclear dipole–dipole interaction has the correct symmetry properties to induce E to A conversion. Terms involving operators such as S_+I_z, S_+I_+ and S_+I_- mediate the tunnel resonance transitions so that resonant contact with the electron spin involves three sets of transitions:

$$\left(\omega_S - \omega_t^{(i)} \pm l\omega_n\right); \quad l = 0, 1 \tag{3}$$

where ω_n is the ^{1}H Larmor frequency. Since the electron spins are well coupled to the lattice this leads to a cooling of the tunnel reservoir.

Transitions labelled $l = 0$ are driven by S_+I_z and lead to no change in ^{1}H polarisation. However, there will be methyl groups that have tunnelling frequencies $\omega_t^{(i^+)} = \omega_t^{(i)} + \omega_n$ and $\omega_t^{(i^-)} = \omega_t^{(i)} - \omega_n$ which will be cooled by the electron via the transitions labelled $l = 1$. These are driven by operators such as S_+I_+ and S_+I_- and do involve changes in ^{1}H polarisation. Here the energy mismatch between $\hbar\omega_t^{(i^\pm)}$ and $\hbar\omega_s$ is made up by the ^{1}H Zeeman energy.

Therefore, adapting Eq. (16) derived by Clough and Hobson [16] to include the tunnel distribution, the rate of change in the ^{1}H polarisation $\langle I_z \rangle$ due to resonant contact with the electron spin when the sample is relaxed at the field B_r may be written as,

$$\frac{1}{I_0}\left[\frac{d\langle I_z\rangle}{dt}\right]_{tr} = a\left(\theta_L^{-1}-\theta_{t(i)}^{-1}\right)\left[W^{(-)}g\left(\omega_S-\omega_t^{(i)}-\omega_n\right) - W^{(+)}g\left(\omega_S-\omega_t^{(i)}+\omega_n\right)\right]G\left(\omega_t^{(i)}\right) \quad (4)$$

where a is a constant. This mechanism is one that can lead to dynamic nuclear polarisation of the ^{1}H spins. Additionally the ^{1}H polarisation will slowly evolve towards equilibrium due to spin–lattice relaxation so another contribution to the rate equation for $\langle I_z\rangle$ is,

$$\left[\frac{d\langle I_z\rangle}{dt}\right]_{rel} = -\frac{(\langle I_z\rangle - I_0)}{T_1} \quad (5)$$

where I_0 is the equilibrium polarisation at the field $B_r$and T_1 is the spin–lattice relaxation time at the same field.

For each value of field, B_r, three sets of tunnelling CH_3 subgroups are cooled. The change in the inverse temperature of the tunnel reservoir associated with CH_3 groups i may be determined by adapting Eq. (18) derived by Clough and Hobson [16] as follows,

$$\frac{d\left(\theta_L^{-1}-\theta_{t(i)}^{-1}\right)}{dt} = -a_t\left(\theta_L^{-1}-\theta_{t(i)}^{-1}\right) \times \begin{bmatrix} W^{(-)}g\left(\omega_S-\omega_t^{(i)}-\omega_n\right) \\ +W^{(+)}g\left(\omega_S-\omega_t^{(i)}+\omega_n\right)+W^{(0)}g\left(\omega_S-\omega_t^{(i)}\right)\end{bmatrix} G\left(\omega_t^{(i)}\right) \quad (6)$$

where $W^{(0,\pm)}$ are transition probabilities per unit time and a_t is a constant.

The tunnel diffusion process promotes equilibration towards a common temperature among the tunnelling subgroups. Conversion of one methyl group between E and A species is accompanied by a second methyl group making the reverse transition. Where the two groups have the same tunnelling frequency the process promotes spatial diffusion. However, spectral diffusion of tunnelling energy can also proceed if the two CH_3 groups have a mismatch in energy which is equal to the ^{1}H Zeeman splitting at that field. Then the difference in tunnelling energy is made up by a flip of the ^{1}H spin and in this case it is the nuclear dipole–dipole interaction that mediates the energy exchange. Consequently the spectral diffusion process is accompanied by a change in ^{1}H nuclear spin polarisation. For two CH_3 tunnelling subgroups the respective heat capacities are proportional to the tunnelling distribution $G(\omega_t)$. The two subgroups will tend towards mutual equilibrium and if the frequency difference between the two matches the ^{1}H Larmor frequency, $\omega_t^{(i)}-\omega_t^{(i^\pm)} = \mp\omega_n$ then the rate of change in tunnelling temperatures of subgroups i and $i^\pm$ will be governed by,

$$\frac{d\theta_{t(i)}}{dt} = -k_d\frac{G\left(\omega_t^{(i)}\right)}{G\left(\omega_t^{(i)}\right)+G\left(\omega_t^{(i^\pm)}\right)}\left(\theta_{t(i)}-\theta_{t(i^\pm)}\right)\delta\left(\omega_t^{(i)}-\omega_t^{(i^\pm)}\pm\omega_n\right)$$
$$\frac{d\theta_{t(i^\pm)}}{dt} = -k_d\frac{G\left(\omega_t^{(i^\pm)}\right)}{G\left(\omega_t^{(i)}\right)+G\left(\omega_t^{(i^\pm)}\right)}\left(\theta_{t(i^\pm)}-\theta_{t(i)}\right)\delta\left(\omega_t^{(i)}-\omega_t^{(i^\pm)}\pm\omega_n\right) \quad (7)$$

where $\delta(\omega)$ is the Kroneker delta function. The tunnel diffusion process between the reservoirs associated with these two subgroups is also accompanied by the change in ^{1}H polarisation; we may write this as follows,

$$\frac{1}{I_0}\left[\frac{d\langle I_z\rangle}{dt}\right]_{td}^{(i,i^\pm)} = k_0\frac{G\left(\omega_t^{(i)}\right)G\left(\omega_t^{(i^\pm)}\right)}{G\left(\omega_t^{(i)}\right)+G\left(\omega_t^{(i^\pm)}\right)}\left(\theta_{t(i)}-\theta_{t(i^\pm)}\right)\delta\left(\omega_t^{(i)}-\omega_t^{(i^\pm)}\pm\omega_n\right) \quad (8)$$

where k_d and $k_0 = 1/T_{diff}$ are constants. Eq. (8) defines the change in ^{1}H polarisation arising from a pair of tunnelling subgroups; the net change in $\langle I_z\rangle$ for the ensemble will be a sum over all subgroups. This diffusion process provides a second DNP mechanism.

Finally, the total change in $\langle I_z\rangle$ arising from each step in the field-cycling sequence is the sum of ESR, diffusion and spin–lattice relaxation terms, Eqs. (4), (5) and (8).

5. Discussion

Eqs. (4)–(7) and (8) define our model for tunnel resonance, comprising rate equations for $\langle I_z\rangle$ and $\theta_{t(i)}$ which include three mechanisms (a) contact with the electron spin, (b) spectral diffusion of tunnelling energy and (c) spin–lattice relaxation. Any dependence of spatial diffusion on the distance between methyl groups is excluded from the current analysis. Numerical simulations based on the model have been used to emulate experimental observations. The basis comprises 101 tunnelling subgroups that define the tunnelling distribution centred on ω_t; each is characterised by $\theta_{t(i)}$ and $\omega_t^{(i)}$. In defining the model, spectrally adjacent reservoirs are separated in frequency by ω_n and these equilibrate via tunnel diffusion, Eq. (7), generating DNP, Eq. (8). The parameters g_{obs}, A_{Cu}, T_1 and I_0 are determined experimentally. The line shapes in the ESR spectrum $g(\omega)$ were defined as Gaussian with HWHM 0.63 mT consistent with ESR spectra reported in Ref. [18]. In the simulations the initial tunnelling temperature was assumed to be 40 K and the lattice temperature was 4.2 K. The transition probabilities $W^{(0)}$, $W^{(+)}$ and $W^{(-)}$ have similar magnitude and for the purposes of this simulation they are assumed to be equal. Therefore for a given Cu^{2+} concentration there are four adjustable parameters $aW^{(\pm)}$, $a_tW^{(0,\pm)}$, k_d and k_0 defined in the differential equations. By comparing the model simulations with the experimental data these were determined to give the best fit to the data and are reported in Table 1.

The simulations of the experiments conducted are represented by solid lines in Figs. 2–5 and they correspond well with the experimental data. The DNP line shapes are reproduced well as are other more subtle effects, for example (a) in Fig. 2 the systematic decline in the amplitudes of the four members of the ESR tunnel resonance spectrum for sample I and (b) in Fig. 3 the hysteresis depending on the direction of the field scan. In Fig. 4 the cooling of the tunnelling reservoir in the three samples is reproduced and in Fig. 5 tunnel diffusion is found to be independent of Cu^{2+} ion concentration. Given a single set of parameters, the consistency in the outcomes of the simulations for the different types of experiments 3.1–3.4 shown in the figures is gratifying.

In Fig. 3 the difference spectrum of up-field and down-field scans results in bell-shaped peaks in both experiment and numerical simulations. This observation suggests that this difference spectrum is dominated by the electron contact term, Eq. (4), as asserted by Clough using an approximate analytical line shape analysis [12,16].

The parameters $aW^{(\pm)}$ and $a_tW^{(0,\pm)}$ determine the strength of the transitions that mediate the contact between the electron spins and the tunnel reservoir. Therefore it is expected that these values will be approximately proportional to the Cu^{2+} ion concentration. This is confirmed in Table 1 where these parameters are found to be proportional to within approximately 15%. By contrast the spin-diffusion mechanism does not depend on the presence of paramagnetic impurities and indeed k_d and k_0 are independent of Cu^{2+} ion concentration.

In Fig. 6 the qualitative features of the polarisation build-up as a function of time is simulated successfully although the quantitative agreement for the data evolved on the negative lobe of the DNP line shape is less good than for the positive lobe. This may

simply reflect a small difference in the transition probabilities for the two lobes which have been assumed equal in the model.

While the changes in ^{1}H polarisation that characterise the tunnel resonance phenomenon can be illustrated well by experimental data shown in Figs. 2–6, we have no direct measurements of the temperatures of the tunnelling reservoirs. To illustrate the model's behaviour in this respect we have plotted the evolution of the tunnelling temperatures in Figs. 7 and 8. A simulation of the scan shown in Fig. 3 is shown in Fig. 7 where the mesh shows the evolution of $\theta_{t(i)}$ as a function of time for sample II. As expected the groups at the centre of the distribution are cooled the most efficiently. Progressing along the time axis, four downward steps in temperature are encountered when the four Cu hyperfine lines in the ESR spectrum successively become resonant with the tunnelling methyl groups. In between each step there is a small recovery in $\theta_{t(i)}$ at the centre of the distribution due to tunnel diffusion. At approximately $t = 3 \times 10^4$ s the field scan is reversed and each of the four Cu hyperfine lines is encountered again and recorded as steps in tunnelling temperature.

In Fig. 8 the effects of tunnel diffusion are recorded in a simulation of the data shown in Fig. 5. Zero time defines the completion of the 1800 s preparation period on the negative lobe of the DNP line shape. Subsequently the plot records the evolution, off tunnel-resonance, at the field $B_r \approx 84$ mT. At time $t = 0$ the effect of inhomogeneous cooling across the tunnelling distribution is evident but with increasing time the different tunnelling sub-groups progressively equilibrate due to tunnel diffusion.

The observed distribution in tunnelling frequencies is relatively small, approximately 2.5% of the central frequency. This may arise in part from the inhomogeneities that are introduced into the potential barriers of different methyl groups due to the doping with Cu^{2+} ions, although there is no evidence in our data that this is dependent on the Cu^{2+} ion concentrations used in our experiments. The sensitivity of tunnelling and potential energy surfaces to the presence of substitutional impurities has been demonstrated by the group of Trommsdorff in their investigations of double proton transfer in the hydrogen bonds of carboxylic acid dimers [20]. Although small in breadth, the tunnelling distribution observed

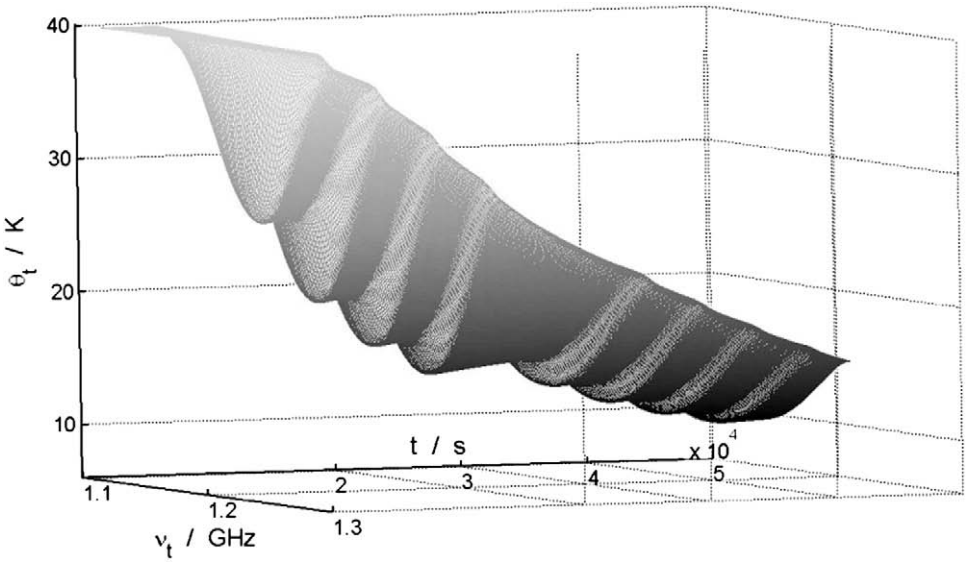

Fig. 7. Numerical simulation of the tunnel resonance experiment shown in Fig. 3 showing the distribution of tunnel temperatures $\theta_{t(i)}$ as a function of time. The figure records a down-field scan followed by an up-field scan.

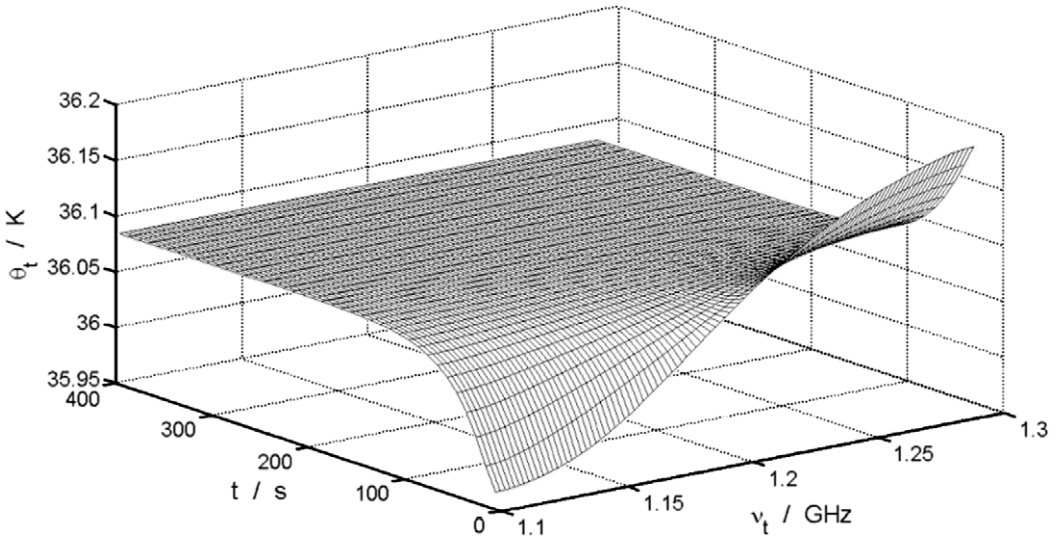

Fig. 8. Numerical simulation of the tunnel diffusion experiment shown in Fig. 5 showing the distribution of tunnel temperatures as a function of time.

in the present study is sufficient to explain the observed DNP effects. Indeed the tunnel distribution is pivotal to the existence of the DNP effect in this case.

6. Concluding remarks

The Pauli Exclusion Principle strongly influences the nuclear spin-symmetry of rotational groups and as a result the associated thermal reservoirs can exhibit strong deviations from thermal equilibrium at low temperature. The tunnel resonance spectra illustrate how the excess energy contained can subsequently be released when brought into resonant contact with an electron spin. The quanta involved may be substantially larger than the nuclear Larmor frequency, nevertheless, various interactions provide coupling to the nuclear spins and we have shown how the subsequent redistribution of energy can lead to large changes in nuclear spin polarisation through DNP. By monitoring the nuclear spin polarisation the mechanisms involved have been explored and the observations have been successfully emulated in a numerical simulation. It is found that the tunnelling diffusion rate is independent of Cu^{2+} ion concentration, *C*, while the processes which directly involve the electron spin are approximately proportional to *C*. The same numerical model is used to describe a range of different observations including: the DNP tunnel resonance line shapes described in Section 3.1; the cooling of the tunnelling reservoir and the *A*–*E* conversion rate on resonance with the electron spin described in Section 3.2; the spectral diffusion of tunnelling energy described in Section 3.3; and the time evolution of the ^1H polarisation in the vicinity of the tunnel resonance described in Section 3.4,. For a given Cu^{2+} concentration, a consistent set of adjustable parameters in the numerical model successfully reproduce these various observations.

Acknowledgments

The construction of the field-cycling spectrometer was financially supported by the Royal Society (Paul Instrument Fund) and the Engineering and Physical Sciences Research Council. We gratefully acknowledge Professor Stan Clough for many stimulating discussions.

References

[1] A. Abragam, M. Goldman, Principles of dynamic nuclear-polarization, Rep. Prog. Phys. 41 (1978) 395–467.
[2] J.H. Ardenkjaer-Larsen, B. Fridlund, A. Gram, G. Hansson, L. Hansson, M.H. Lerche, R. Servin, M. Thaning, K. Golman, Increase in signal-to-noise ratio of >10,000 times in liquid-state NMR, Proc. Natl. Acad. Sci. USA 100 (2003) 10158–10163.
[3] D.A. Hall, D.C. Maus, G.J. Gerfen, S.J. Inati, L.R. Becerra, F.W. Dahlquist, R.G. Griffin, Polarization-enhanced NMR spectroscopy of biomolecules in frozen solution, Science 276 (1997) 930–932.
[4] C.G. Joo, K.N. Hu, J.A. Bryant, R.G. Griffin, In situ temperature jump high-frequency dynamic nuclear polarization experiments: enhanced sensitivity in liquid-state NMR spectroscopy, J. Am. Chem. Soc. 128 (2006) 9428–9432.
[5] M. Prager, A. Heidemann, Rotational tunneling and neutron spectroscopy: a compilation, Chem. Rev. 97 (1997) 2933.
[6] H. Glättli, A. Sentz, M. Eisenkremer, Conversion of spin species in solid CH_4 through level crossing with paramagnetic impurities, Phys. Rev. Lett. 28 (1972) 871.
[7] P. Van Hecke, G. Janssens, NMR direct detection of tunnel splittings in solid SiH_4, Phys. Rev. B 17 (1978) 2124.
[8] A.J. Horsewill, Quantum tunnelling aspects of methyl group rotation studied by NMR, Prog. Nucl. Magn. Reson. Spectrosc. 35 (1999) 359–389.
[9] B.S. Bharaj, M.M. Pintar, Saturation of molecular rotational tunneling doublet by hot nuclear spins: a method for measuring tunneling spectrum, Phys. Rev. Lett. 52 (1984) 1986–1989.
[10] G. Vandemaele, P. Coppens, L. Van Gerven, New method to study spin conversion of a nuclear-spin rotor with low tunnel splitting, Phys. Rev. Lett. 56 (1986) 1202–1205.
[11] S. Clough, A. Heidemann, M. Paley, The temperature dependence of methyl tunnelling motion in three acetates, J. Phys. C Solid State Phys. 14 (1981) 1001–1008.
[12] S. Clough, A.J. Horsewill, M.N.J. Paley, Diffusion of methyl-group tunneling energy, Phys. Rev. Lett. 46 (1981) 71–74.
[13] S. Clough, B.J. Mulady, Tunneling resonances in proton spin–lattice relaxation, Phys. Rev. Lett. 30 (1973) 161–163.
[14] S. Clough, W.S. Hinshaw, T. Hobson, Nuclear-spin-symmetry conversion of tunneling methyl groups, Phys. Rev. Lett. 31 (1973) 1375–1377.
[15] S. Clough, A.J. Horsewill, M.N.J. Paley, Dynamic nuclear polarisation by the cooling of tunnelling methyl groups, J. Phys. C Solid State Phys. 15 (1982) 3803–3808.
[16] S. Clough, T. Hobson, Tunnelling magnetic resonances, J. Phys. C Solid State Phys. 7 (1974) 3387–3402.
[17] F. Noack, NMR field-cycling spectroscopy – principles and applications, Prog. Nucl. Magn. Reson. Spectrosc. 18 (1986) 171–276.
[18] N.M. Atherton, A.J. Horsewill, An electron-spin-resonance and proton ENDOR study of copper-doped zinc acetate dihydrate, Mol. Phys. 42 (1981) 985–997.
[19] D.L. Noble, I. Frantsuzov, A.J. Horsewill, Field-cycling NMR investigations of ^{13}C–^1H cross-relaxation and cross-polarisation: the nuclear solid effect and dynamic nuclear polarisation, Solid State Nucl. Magn. Reson. 34 (2008) 110–117.
[20] A. Oppenländer, C. Rambaud, H.P. Trommsdorff, J.C. Vial, Translational tunneling of protons in benzoic acid crystals, Phys. Rev. Lett. 63 (1989) 1432–1435.